Nonlinear Finite-Difference Time-Domain Method for the Simulation of Anisotropic, $\chi^{(2)}$, and $\chi^{(3)}$ Optical Effects

Charles M. Reinke, *Student Member, IEEE,* Aliakbar Jafarpour, Babak Momeni, *Student Member, IEEE,* Mohammad Soltani, Sina Khorasani, Ali Adibi, *Senior Member, IEEE,* Yong Xu, and Reginald K. Lee, *Member, IEEE*

***Abstract*—A two-dimensional (2-D) finite-difference time-domain (FDTD) code for the study of nonlinear optical phenomena, in which both the slowly varying and the rapidly varying components of the electromagnetic fields are considered, has been developed. The algorithm solves vectorial Maxwell's equations for all field components and uses the nonlinear constitutive relation in matrix form as the equations required to describe the nonlinear system. The stability of the code is discussed and its effectiveness is demonstrated through the simulations of self-phase modulation (SPM) and second-harmonic generation (SHG). The authors also show that the combination of nonlinear effects with PCs can result in a significant improvement in device size and integrability, using the example of a Mach–Zehnder interferometer (MZI).**

***Index Terms*—Finite-difference time domain, nonlinear optics, photonic crystals.**

I. Introduction and Motivation

NONLINEAR optics has a wide range of applications in many areas such as communications and optical computing [1]. Of particular interest, we can use nonlinear optical materials to achieve all-optical control of electromagnetic waves, which can lead to all-optical signal processing. Nonlinear optics also has a number of inherent benefits, such as the ability to compensate for linear dispersion and diffraction effects, as evidenced by temporal and spatial solitons [2]. Utilizing the nonlinear properties of various materials, optical switches and modulators have also been realized and found wide applications in modern telecommunication industry [3], [4].

Recently, photonic crystal (PC) structures have also been extensively investigated in literature [5]–[10]. One of the most unique features of PC structures is that for a large enough index contrast, a PC can exhibit a photonic bandgap, i.e., a range of frequencies within which a propagating electromagnetic wave does not exist [11]–[15]. More practically, PC structures are also interesting, because they allow for precise control of electromagnetic wave propagation, as exemplified in the studies of sharp bends [16], nanoscale optical cavities [17], and add–drop filters [18]. Since PC structures can support electromagnetic modes with unique modal profiles and drastically differing dispersion properties, the introduction of nonlinear materials into PC structures has led to many interesting nonlinear optical phenomena [19]–[32]. Furthermore, it is possible to achieve a greatly reduced group velocity for guided modes in PC structures, which can significantly improve the efficiency of nonlinear optical processes in such structures due to slow-light enhancement [33]. As a result, it is of critical importance to develop a numerical algorithm that can easily and accurately simulate nonlinear optical process in complex dielectric structures such as PCs.

A very common technique for the analysis of nonlinear optical wave propagation is the nonlinear Schrödinger equation. The solutions of the nonlinear Schrödinger equation can be found analytically, which provide the basic framework for the investigation of important subjects such as temporal and spatial solitons [34] and can lend important insights for the study of other nonlinear optical phenomena [35], [36]. Unfortunately, it is generally difficult to apply the nonlinear Schrödinger equation to describe nonlinear wave propagation in PCs, since PC structures typically have very large index contrast and exhibit significant modal dispersion (especially near the band edge), which invalidates some basic approximations in the derivation of the nonlinear Schrödinger equation [37].

The finite-difference time-domain (FDTD) method of analysis [38], however, is applicable for a wide range of complex dielectric structures, constrained only by the size of the computational space required for the simulation. Several FDTD-based algorithms have been developed to address nonlinear phenomena, including an FDTD formulation by Sullivan [39] for nonlinear dispersive optical structures that utilizes Z transforms. However, most of these methods either use relatively complex formulations solved using iterative techniques [40], [41] or simplify the problem by neglecting certain field components [42] at the expense of a lost generality. In fact, a three-dimensional (3-D) FDTD-based $\chi^{(3)}$ nonlinear code that uses an iterative technique and parallel algorithms has been

Manuscript received November 12, 2004; revised September 9, 2005. This work was supported by the Office of Naval Research (J. Meyer), the Air Force Office of Scientific Research (G. Pomrenke), and by the Southeastern Center for Electrical Engineering Education.

C. M. Reinke, A. Jafarpour, B. Momeni, M. Soltani, S. Khorasani, and A. Adibi are with the School of Electrical and Computer Engineering, Georgia Institute of Technology, Atlanta, GA 30332-0250 USA (e-mail: adibi@ece.gatech.edu).

Y. Xu is with the Department of Electrical and Computer Engineering, Virginia Polytechnic Institute and State University, Blacksburg, VA 24061 USA.

R. K. Lee is with the Department of Applied Physics, California Institute of Technology, Pasadena, CA 91125 USA.

Digital Object Identifier 10.1109/JLT.2005.859835

demonstrated [43]–[47], but for many problems, a quick 2-D simulator is both desirable and sufficient. Although a practical FDTD code that can solve all nonlinear problems is elusive at best, the problem is not intractable, and for the case of Kerr media, a simple and robust solution may be found, as shown by Tran [48], [49].

In this paper, we present a 2-D FDTD code for simulating nonlinear effects in anisotropic materials and $\chi^{(2)}$ and $\chi^{(3)}$ materials of practical interest. This code has been optimized by focusing only on the materials of interest and by assuming that the nonlinear effects are instantaneous. Thus, it offers better computational efficiency over other nonlinear FDTD methods, at the expense of a small loss of generality in application. The stability of the code is demonstrated and several simulation results are offered. This discussion begins with an overview of the basic FDTD algorithm and a description of our nonlinear extension to the original linear method, discussed in Section II. Here, the techniques used to calculate anisotropic, $\chi^{(2)}$, and $\chi^{(3)}$ nonlinearities are presented, as well as the limitations of each case. A straightforward analysis of the stability of our code under the linear conditions is given in Section III. The code is verified in Section IV, using the well-studied bulk nonlinear phenomenon of second-harmonic generation (SHG) and self-phase modulation (SPM). Furthermore, the simulation of a simple nonlinear PC is presented along with a specific PC application utilizing the SPM effect. Final conclusions are made in Section V.

II. Extension of Yee's FDTD Algorithm

The 2-D FDTD method that we developed is based on a modification of the original Yee's FDTD algorithm [38]. The original FDTD approach solves the coupled linear Maxwell's equations in differential form, written as

$$\frac{\partial}{\partial t}\mathbf{H} = -\frac{1}{\mu}\nabla \times \mathbf{E} \tag{1}$$

$$\frac{\partial}{\partial t}\mathbf{E} = +\frac{1}{\varepsilon}\nabla \times \mathbf{H} \tag{2}$$

where the permittivity ε and the magnetic permeability μ are both time-independent scalars. By discretizing the simulation domain into a finite computational grid, the magnetic and electric fields are computed at interlacing time intervals, as shown here for the x components

$$\begin{aligned} H_x^{n+\frac{1}{2}}&\left(i, j+\frac{1}{2}, k+\frac{1}{2}\right) \\ &= H_x^{n-\frac{1}{2}}\left(i, j+\frac{1}{2}, k+\frac{1}{2}\right) \\ &\quad + \frac{\Delta t}{\mu}\left(\frac{E_y^n\left(i, j+\frac{1}{2}, k+1\right) - E_y^n\left(i, j+\frac{1}{2}, k\right)}{\Delta z}\right. \\ &\qquad \left. - \frac{E_z^n\left(i, j+1, k+\frac{1}{2}\right) - E_z^n\left(i, j, k+\frac{1}{2}\right)}{\Delta y}\right) \end{aligned} \tag{3}$$

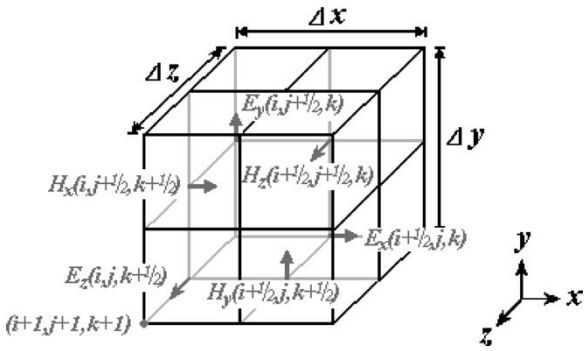

Fig. 1. Traditional Yee's cell for the FDTD field components, showing the spatial relationship between the x, y, and z components of the electric field $\mathbf{E}$, and the magnetic field $\mathbf{H}$. Here, i, j, and k represent the grid indices in the x-, y-, and z-directions, respectively.

$$\begin{aligned} E_x^{n+1}&\left(i+\frac{1}{2}, j, k\right) \\ &= E_x^n\left(i+\frac{1}{2}, j, k\right) \\ &\quad - \frac{\Delta t}{\varepsilon}\left(\frac{H_y^n\left(i+\frac{1}{2}, j, k+\frac{1}{2}\right) - H_y^n\left(i+\frac{1}{2}, j, k-\frac{1}{2}\right)}{\Delta z}\right. \\ &\qquad \left. - \frac{H_z^n\left(i+\frac{1}{2}, j+\frac{1}{2}, k\right) - H_z^n\left(i+\frac{1}{2}, j-\frac{1}{2}, k\right)}{\Delta y}\right) \end{aligned} \tag{4}$$

where n represents the time index, Δt is the time step, Δy and Δz are the grid spacings in the y- and z-directions, respectively, and i, j, and k are the grid coordinates in the x-, y-, and z-directions, respectively. The y and z field components are calculated from similar equations, with the spatial orientations of these field components as shown in Fig. 1, commonly referred to as the Yee's cell.

In our nonlinear version, the first set of equations in (3) is retained, while the second set of equations is written as

$$\begin{aligned} D_x^{n+1}&\left(i+\frac{1}{2}, j, k\right) \\ &= D_x^n\left(i+\frac{1}{2}, j, k\right) \\ &\quad - \Delta t\left(\frac{H_y^n\left(i+\frac{1}{2}, j, k+\frac{1}{2}\right) - H_y^n\left(i+\frac{1}{2}, j, k-\frac{1}{2}\right)}{\Delta z}\right. \\ &\qquad \left. - \frac{H_z^n\left(i+\frac{1}{2}, j+\frac{1}{2}, k\right) - H_z^n\left(i+\frac{1}{2}, j-\frac{1}{2}, k\right)}{\Delta y}\right) \end{aligned} \tag{5}$$

where D_x^n is the electric displacement in the x-direction, which is known through the nonlinear constitutive relation $\mathbf{D}^n = f(\mathbf{E}^n)(\mathbf{E}^n)$ (f here represents a function). After finding $\mathbf{D}^{n+1}$, the electric field is advanced from the inverse constitutive relation, i.e., $\mathbf{E}^{n+1} = f^{-1}(\mathbf{D}^{n+1})(\mathbf{D}^{n+1})$. This inversion process is possible either through exact analytical methods or an iterative approach starting with $\mathbf{E}^n$ as the initial value. The general

procedure is the same for the cases of anisotropic, second-order $\chi^{(2)}$ nonlinear, and third-order $\chi^{(3)}$ nonlinear media, although the exact implementation in each case has been optimized for computational performance.

Although the $\chi^{(2)}$ and $\chi^{(2)}$ susceptibilities are generally a second- and third-rank tensor, respectively, for a wide variety of materials (such as many of the semiconductors used in modern optoelectronics), most of the tensor elements are negligible or equal to each other due to material symmetries and other considerations. Therefore, the total number of independent tensor elements is significantly reduced. As an example, the general second-order nonlinear susceptibility tensor is commonly written in contracted form as

$$d = \begin{bmatrix} d_{11} & d_{12} & d_{13} & d_{14} & d_{15} & d_{16} \\ d_{21} & d_{22} & d_{23} & d_{24} & d_{25} & d_{26} \\ d_{31} & d_{32} & d_{33} & d_{34} & d_{35} & d_{36} \end{bmatrix} \tag{6}$$

where $d_{ij} = (1/2)\chi^{(2)}_{ij}$, and the indexes i and j are in Voigt notation. However, for $\chi^{(2)}$ materials of interest addressed in this paper, the tensor is simplified as

$$d = \begin{bmatrix} 0 & 0 & 0 & d_{14} & 0 & 0 \\ 0 & 0 & 0 & 0 & d_{25} & 0 \\ 0 & 0 & 0 & 0 & 0 & d_{36} \end{bmatrix} \tag{7}$$

and $d_{14} = d_{25} = d_{36}$ (e.g., $43m$ symmetry). Thus, we only need to consider one independent parameter. In the case of $\chi^{(3)}$ materials, the tensor has many more elements and may not be easily written; however, we can apply the same simplification. Thus, many materials used in nonlinear optics have nonlinear susceptibilities that can be treated as a scalar quantity; these are the materials treated by this study. Some examples of $\chi^{(2)}$ and $\chi^{(3)}$ materials of interest include most semiconductors including gallium arsenide, KD*P, and liquid crystals. Note that there are nonlinear algorithms that are capable of treating tensors [50], however, these more complex methods have been developed for systems that require the full tensor forms and do not provide significant benefits for materials such as those used for practical PC applications.

In the case of simple anisotropy, the inverse relation involves the direct inversion of the permittivity matrix. The equations for the inversion of this 3×3 matrix were found explicitly using linear algebra and then implemented directly into Yee's algorithm. For simple nondispersive $\chi^{(2)}$ and $\chi^{(3)}$ nonlinear materials, the required time-dependent (since $\mathbf{E}$ is a function of time) tensors can be actually found from the equivalent constitutive relations given by

$$\mathbf{D} = \varepsilon_0 \begin{bmatrix} \varepsilon_r & 0 & \chi^{(2)}\mathbf{E}\cdot\hat{y} \\ \chi^{(2)}\mathbf{E}\cdot\hat{z} & \varepsilon_r & 0 \\ 0 & \chi^{(2)}\mathbf{E}\cdot\hat{x} & \varepsilon_r \end{bmatrix} \mathbf{E} \tag{8}$$

$$\mathbf{D} = \varepsilon_0 \begin{bmatrix} \varepsilon_r + \chi^{(3)}|\mathbf{E}|^2 & 0 & 0 \\ 0 & \varepsilon_r + \chi^{(3)}|\mathbf{E}|^2 & 0 \\ 0 & 0 & \varepsilon_r + \chi^{(3)}|\mathbf{E}|^2 \end{bmatrix} \mathbf{E} \tag{9}$$

respectively, where $\hat{x}$, $\hat{y}$, and $\hat{z}$ represent unit vectors in the x-, y-, and z-directions, respectively. Although these relations take more elaborate tensor forms in the most general case, this compact notation is both mathematically consistent for the simple materials of interest and also convenient for the rest of this discussion. For $\chi^{(2)}$ nonlinear media, the inverse relation is complicated to the extent that the iterative approach becomes more efficient. In this case, the value of the $\mathbf{E}$ field at a given time step is found from an implicit expression where the value from the previous time step is used as an initial guess for the updated value [51]. The newly calculated value is then used as the next guess, and so on until $\mathbf{E}$ is found to the desired precision. Usually, this process converges after only a few iterations have been completed. For self-focusing $\chi^{(3)}$ nonlinear media where the nonlinear polarization term is essentially a scalar, an inversion function $g = f^{-1}$ may be found in closed form using algebraic techniques [such that $\mathbf{E} = g(D)(\mathbf{D})$], which after simplification results in

$$g\left(\varepsilon_r, \chi^{(3)}, D\right) = \frac{-\sqrt[3]{12}\varepsilon_r + \left(9\sqrt{\chi^{(3)}}D + \sqrt{12\varepsilon_r^3 + 81\chi^{(3)}D^2}\right)^{\frac{2}{3}}}{\sqrt[3]{18\left(9\sqrt{\chi^{(3)}}D + \sqrt{12\varepsilon_r^3 + 81\chi^{(3)}D^2}\right)D\sqrt{\chi^{(3)}}}} \tag{10}$$

in which $D = |\mathbf{D}|$ (i.e., the magnitude of vector $\mathbf{D}$), and ε_r is the local relative permittivity of the medium. Using the above expression, exact evaluation of the inverse constitutive relation becomes possible, and the efficiency of the algorithm is improved by about 30% as compared with the iterative approach. Although the exact improvement in efficiency will depend on computer architecture, programming language, etc., this approach, in general, will be equal to or faster than the iterative approach, since at least one iteration that involves roughly the same number of calculations as (10) must be performed for each grid point during each time step.

In our algorithm, we ignore the frequency dependence of the second-order or third-order nonlinear coefficients. This assumption is well justified if the optical frequency is far from the absorption resonance of the nonlinear materials [52]. Furthermore, the frequency bandwidth of the optical signals is typically much smaller than the dispersion of the nonlinear coefficients, which allows us to treat the $\chi^{(2)}$ or $\chi^{(3)}$ coefficients as frequency-independent constants.

Since the algorithm simulates the behavior of a nonlinear system, the absolute amplitude of the electromagnetic wave in our simulation carries physical meaning and cannot be normalized arbitrarily. We introduce a normalization factor $A_{I,N}$ that relates the physical electric field E and the normalized electric field E_N as $E_N = E/\sqrt{A_{I,N}}$. Correspondingly, the material $\chi^{(2)}$ and $\chi^{(3)}$ nonlinear coefficients are normalized as

$$\chi^{(2)}_N = \chi^{(2)}\sqrt{A_{I,N}} \tag{11}$$

$$\chi^{(3)}_N = \chi^{(3)}A_{I,N} = n_2\frac{cn_0^2}{\pi}A_{I,N} \tag{12}$$

where n_0 is the linear refractive index, n_2 is the second-order nonlinear refractive index, and $\chi^{(2)}_N$ and $\chi^{(3)}_N$ represent the normalized $\chi^{(2)}$ and $\chi^{(3)}$ nonlinear coefficients, respectively.

The renormalization of these quantities is necessary in order to prevent the numerical values from approaching the upper or lower precision limits for a given computer architecture. We should point out that the numerical results given by the FDTD correspond to the normalized values, which can be converted into physical values by using the appropriate normalization factor $A_{I,N}$. Also notice that according to (11) and (12), the normalized nonlinearity coefficients are directly related to both the physical nonlinearity strength and the normalization factor. Thus, materials of various nonlinear strengths or different input intensity levels may be simulated by choosing appropriate values of the normalized nonlinearity strength. As an example of how physical nonlinear values compare with the corresponding normalized quantities, a value of 9.2×10^{-9} (esu) for $\chi^{(2)}$ (beta barium borate) with $A_{I,N} = 1$ corresponds to a normalized $\chi^{(2)}$ of 3.9×10^{-10}, and a value of 4×10^{-14} cm^2/W for n_2 (maximum for GaAs) with $A_{I,N} = 1$ corresponds to a normalized $\chi^{(3)}$ of 5.5×10^{-15}.

The FDTD implementation was coded for two-dimensional (2-D) simulations with rectangular computational domains. At the four computational boundaries, either periodic Bloch [53], perfectly matched layer (PML) [54], or a combination of the two boundary conditions can be specified, depending on the dielectric structure under consideration. The developed code was written in C running under a Tcl/Tk shell on a Linux platform. The efficiency of the nonlinear version, defined as the computation time for a given structure, is measured to be roughly half that of the original linear version. To the best of our knowledge, this is the first report of an efficient 2-D nonlinear FDTD code that handles anisotropic, $\chi^{(2)}$, and $\chi^{(3)}$ media. The basic $\chi^{(3)}$ method is similar to that of Chen and Kim [55], who presented a 2-D FDTD code for $\chi^{(3)}$ materials only. This study additionally includes a discussion of stability issues for the anisotropic, $\chi^{(2)}$, and $\chi^{(3)}$ codes, presented in the next section.

III. Linear Stability

It can be shown that Yee's FDTD algorithm is stable under the Courant's stability condition [56], asserting that the numerical propagation velocity must be greater than the maximum phase velocity of the light in the structure [57]

$$\frac{1}{\Delta t\sqrt{(\Delta x)^{-2}+(\Delta z)^{-2}}} \geq \sup\left\{\frac{1}{\sqrt{\mu_0\varepsilon_0\varepsilon_r}}\right\} = c_{\max}. \quad (13)$$

Notice that this derivation is performed for the 2-D case. This condition is both necessary and sufficient for numerical stability in an FDTD code that only considers linear effects. The extension to anisotropic materials has an almost identical stability condition

$$\frac{1}{\Delta t\sqrt{(\Delta x)^{-2}+(\Delta z)^{-2}}} \geq \sup\left\{\frac{1}{\sqrt{\mu_0\varepsilon_0\,|\mathrm{eig}\{\bar{\bar{\varepsilon}}_r\}|}}\right\} = c_{\max} \quad (14)$$

except that, now, the eigenvalues of the permittivity tensor $\bar{\bar{\varepsilon}}_r$ are considered in the expression.

In order to examine the stability of the nonlinear FDTD implementation, suppose the simulation is run for a given time step and spatial grid size, and the output field is observed over the entire structure. Assuming that the input field is kept unchanged, the simulation must produce the same results as if the time-dependent linear systems were solved with the permittivity being a suitably defined anisotropic time-dependent tensor rather than the original nonlinear case. This is because in Maxwell equations for anisotropic media (and, therefore, the FDTD method also), field components can be decomposed into a superposition of plane waves along various directions. Each direction is normally associated with two eigenvalues and two eigenvectors, which characterize the corresponding eigenmodes. Generally, these two modes propagate at different phase velocities, and if for each direction, the fast mode is stabilized in the numerical scheme, so would be the slower mode. It can be easily demonstrated that the fastest propagating wave corresponds to the smallest refractive index, which must be one of the eigenvalues of the refractive index matrix of the anisotropic medium [58]. Therefore, it is sufficient to consider only the eigenindexes.

For both $\chi^{(2)}$ and $\chi^{(3)}$ nonlinearity, the constitutive relationships, i.e., (8) and (9), respectively, depend on the strength of the electric field at each grid point in the computation space, which makes the stability analysis more complicated than the linear or simple anisotropic cases. In particular, for $\chi^{(2)}$ media, the eigenvalues are

$$\mathrm{eig}\{\bar{\bar{\varepsilon}}\} = \begin{bmatrix} \varepsilon_r + \chi^{(2)}\widetilde{E} \\ \varepsilon_r - \frac{1}{2}(1+j\sqrt{3})\chi^{(2)}\widetilde{E} \\ \varepsilon_r - \frac{1}{2}(1-j\sqrt{3})\chi^{(2)}\widetilde{E} \end{bmatrix} \quad (15)$$

where $\widetilde{E} = \sqrt[3]{(\mathbf{E}\cdot\hat{x})(\mathbf{E}\cdot\hat{y})(\mathbf{E}\cdot\hat{z})}$ and satisfies

$$|\widetilde{E}| = \left|\sqrt[3]{(\mathbf{E}\cdot\hat{x})(\mathbf{E}\cdot\hat{y})(\mathbf{E}\cdot\hat{z})}\right| \leq \frac{|\mathbf{E}|}{\sqrt{3}}. \quad (16)$$

From this expression, we can deduce that for positive values of $\chi^{(2)}$ and assuming that the strength of the nonlinearity is not greater than a defined limit, the Courant's stability condition will suffice, where the limit requires that $|\chi^{(2)}\tilde{E}| < \varepsilon_r$ as shown here:

$$\begin{aligned} \widetilde{E} > 0:\ \min\{|\mathrm{eig}\{\bar{\bar{\varepsilon}}\}|\} &= \sqrt{\varepsilon_r^2 + (\chi^{(2)}\widetilde{E})^2 - \varepsilon_r\chi^{(2)}\tilde{E}} \\ &\geq \varepsilon_r - \chi^{(2)}|\widetilde{E}| \geq \varepsilon_r - \chi^{(2)}\frac{|\mathbf{E}|}{\sqrt{3}} \\ \widetilde{E} < 0:\ \min\{|\mathrm{eig}\{\bar{\bar{\varepsilon}}\}|\} &= \varepsilon_r - \chi^{(2)}|\widetilde{E}| \geq \varepsilon_r - \chi^{(2)}\frac{|\mathbf{E}|}{\sqrt{3}}. \end{aligned} \quad (17)$$

Therefore, for sufficiently large nonlinearity, as a result of either large field amplitudes or large normalized $\chi^{(2)}$ values, the smallest eigenvalue tends to zero and the Courant's condition no longer guarantees stability [see (14)]. In other words, for nonlinearity strengths and field values that are not too large (i.e., $|\chi^{(2)}\widetilde{E}| < \varepsilon_r$), the linear stability constraints on the time step size are sufficient. However, for large nonlinearity strength or

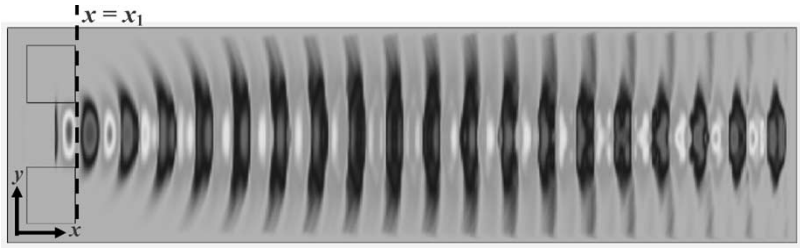

Fig. 2. Self-focusing of a beam radiating out of a dielectric slab waveguide by using a bulk $\chi^{(3)}$ nonlinear medium. The structure for $x < x_1$ represents a slab waveguide with dielectric core ($\varepsilon_r = 12.96$) and air cladding. The structure for $x > x_1$ is a bulk nonlinear medium with $\varepsilon_r = 12.96$ and normalized $\chi^{(3)} = 1$. The fundamental guided mode of the slab waveguide is excited using a Huygens' source, and the structure is surrounded by PML boundaries. The spatial pattern of the electric field throughout the structure calculated by the nonlinear 2-D FDTD method is shown, demonstrating the self-focusing effect.

field values, a smaller time step should be used to guarantee that stability is maintained, as seen in (17). In fact, while stable operation has been demonstrated using normalized $\chi^{(2)}$ values as large as 10, instability has also been encountered for certain simulations using normalized $\chi^{(2)}$ of only 5. The difference between the two cases is the maximum field intensity encountered in the structure, which, for the case of cavities or similar resonant structures, can have localized spikes that increase risk of instability over that of a slab of bulk material, for example. Furthermore, Taflove and Hagness [52] reported encountering similar stability problems with their $\chi^{(2)}$ nonlinear implementations of the FDTD method.

The stability argument for $\chi^{(3)}$ materials of interest is considerably simpler than the $\chi^{(2)}$ case, primarily since we are mainly studying self-focusing media and the corresponding tensor is isotropic. In this case, an analysis of the minimum value taken by the eigenvalues of the constitutive matrix shows that for any positive values of $\chi^{(3)}$ (i.e., for any positive Kerr materials), Courant's stability condition is still sufficient for code stability

$$\min\{\mathrm{eig}\{\bar{\bar{\varepsilon}}\}\} = \varepsilon_r + \chi^{(3)}|\mathbf{E}|^2 \geq \varepsilon_r, \qquad \chi^{(3)} \geq 0. \tag{18}$$

Therefore, the linear stability condition is applicable, since the self-focusing effect results in a local decrease of phase velocity. As verification of this statement, a more detailed calculation for the scalar transverse electric (TE) modes in self-focusing media may be performed [59], which results in

$$\frac{\sqrt{\frac{\partial\left[\varepsilon_r E + \chi^{(3)}E^3\right]}{\varepsilon_r \partial E}}}{\Delta t\sqrt{(\Delta x)^{-2} + (\Delta z)^{-2}}} \geq \frac{1}{\Delta t\sqrt{(\Delta x)^{-2} + (\Delta z)^{-2}}} \geq c_{\max}. \tag{19}$$

Clearly, the same result is reached, confirming that Courant's stability condition is sufficient for $\chi^{(3)}$ nonlinearity in the materials of interest in which only one independent $\chi^{(3)}$ component exists.

IV. Application Examples

A. Bulk Structures

In order to validate the nonlinear FDTD code described in the previous sections, two types of well-understood nonlinear optical phenomena were simulated, namely: 1) self-focusing of optical beams in $\chi^{(3)}$ nonlinear media and 2) SHG in $\chi^{(2)}$ materials. In these simulations, we use a Huygens source [60] to excite a propagating wave that originates from a conventional dielectric slab waveguide and continues through the nonlinear dielectric medium. In Fig. 2, the electric field profile of such a propagating wave is shown for the case of a bulk $\chi^{(3)}$ material with normalized $\chi^{(3)} = 1$. As shown in the figure, the wave is excited by the Huygens source at the location $x = x_1$ and propagates from left to right in the nonlinear medium. A qualitative observation of the diagram indicates that the lensing effect of the material focuses an initially divergent beam and causes the light to converge when the beam arrives at the end of the computational domain.

The numerical verification of our $\chi^{(3)}$ nonlinear code was performed using the well-known formula for the phenomenon of SPM. The index of refraction n is the square root of the permittivity, which, in this case, may be written as

$$n = n_0 + \delta n = \sqrt{\varepsilon_r + \chi^{(3)}|\mathbf{E}|^2} \approx n_0 + \frac{\chi^{(3)}}{2\sqrt{\varepsilon_r}}|\mathbf{E}|^2 \tag{20}$$

where ε_r is the relative permittivity, and n_0 is the linear refractive index. SPM arises from the δn term, which changes the local effective index of the material in proportion to the square of the electric field strength.

If we consider a plane wave incident upon a material exhibiting third-order nonlinearity, we find that for a TE-polarized wave (i.e., electric field normal to the 2-D computation plane, which is the $x-y$ plane), the z component of the electric field has the form

$$E_z = A\cos(kx + \phi) = A\cos(\omega n x + \phi) \tag{21}$$

where A is the amplitude, k is the wavenumber, ω is the angular frequency, x is the position along the propagation direction, and φ is a phase constant. Here, we normalize the speed of light in vacuum to $c = 1$. In our simulations, the unidirectional traveling wave excited by the Huygens source can be well approximated by a plane wave near the right end of the computational domain, as seen in Fig. 3. If we neglect φ for the moment, which is valid as long as the nonlinear field component is relatively weak, we can take the second derivative of E_z and approximately find

$$\frac{dE_z}{dx} = -\omega n A\sin(\omega n x)$$
$$\frac{d^2E_z}{dx^2} = -\omega^2 n^2 A\cos(\omega n x). \tag{22}$$

Fig. 3. Structure used to produce plane-wave excitation of bulk nonlinear $\chi^{(3)}$ material for numerical SPM verification. The structure for $x < x_1$ represents a slab waveguide with dielectric core ($\varepsilon_r = 12.96$) and air cladding. The structure for $x > x_1$ is a bulk linear medium with $\varepsilon_r = 12.96$. The fundamental guided mode of the slab waveguide is excited using a Huygens' source, and the structure is surrounded by PML boundaries. The spatial pattern of the electric field throughout the structure calculated by the linear 2-D FDTD method is shown, with a plane-wave-like pattern produced at the rightmost end of the domain.

We may then divide the second derivative by the original field and take the square root and write

$$n = \sqrt{\frac{-\frac{d^2 E_z}{dx^2}}{\omega^2 E_z}}. \tag{23}$$

Shifting of the calculated values due to the phase constant and discrete differentiation may be accounted for by considering the peaks of the numerator and denominator terms under the square root, shown as

$$n = \sqrt{\frac{\max\left(-\frac{d^2 E_z}{dx^2}\right)}{\max(\omega^2 E_z)}}. \tag{24}$$

An additional issue that must be accounted for is the extra harmonic components present in E_z for the nonlinear case [61], which likely result from the fact that the spatial variation of the phase term ϕ can no longer be ignored when large values are chosen for $\chi^{(3)}$. The electric field in this case is not perfectly sinusoidal, resulting in considerable distortion of the calculated second derivative. This extra harmonic effect is shown in Fig. 4(a), which depicts the variation of E_z and $-d^2E_z/dx^2$ with the FDTD grid position (or x) at a fixed time within a $\chi^{(3)}$ material with normalized $\chi^{(3)} = 4$ (the field values were normalized to 1). This can be overcome by filtering the field values using a low-pass filter such that only the fundamental harmonic component remains, as shown in Fig. 4(b), which displays the same functions as in Fig. 4(a) after the filtering process has been applied.

Using (20), δn may now be calculated by subtracting the value of the linear refractive index from the refractive index obtained numerically from (24). Notice that the maximum of the squared E_z values from the FDTD simulation results was used in the calculation, although the average value is assumed in the theoretical analysis; the average field intensity can be related to the maximum field intensity through

$$\left\langle |\mathbf{E}|^2 \right\rangle = \frac{|\mathbf{E}|^2_{\max}}{2}. \tag{25}$$

Comparing the simulation results (24) with the analytical expression for n (20), we find agreement to within 12% error. We may also compare the permittivity values directly, eliminating the approximation used to separate the square-root terms in (20). The values using this approach agree to within only 2.6% error, much smaller due to the fact that the error in truncation of the binomial expansion of (20) is no longer ignored. Since it is commonly understood that the FDTD in practical usage has a typical error of a few percent, these results verify within reasonable agreement the accuracy of our third-order nonlinear code.

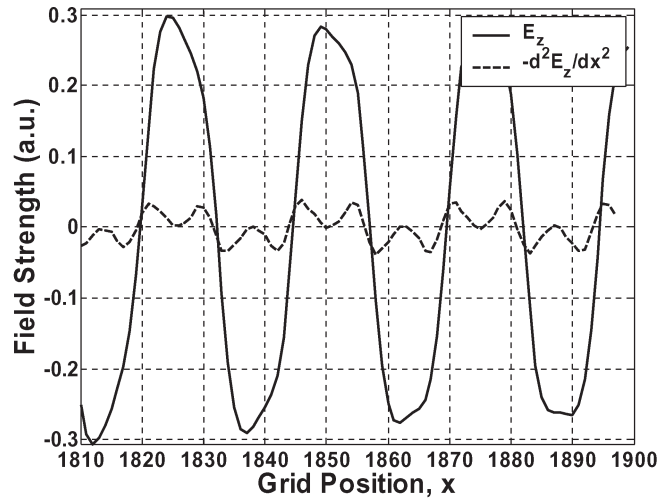

(a)

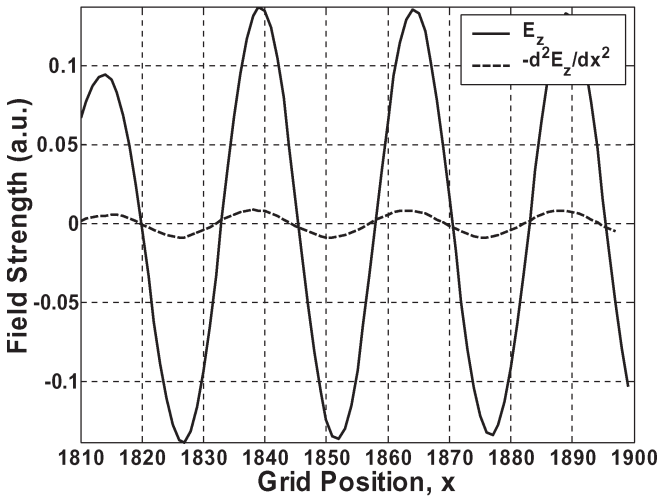

(b)

Fig. 4. (a) Variation of the out-of-plane (or z) component of the electric field (E_z) calculated using the nonlinear FDTD method and its second derivative with position (x) along the guiding direction within a $\chi^{(3)}$ nonlinear bulk material with normalized $\chi^{(3)} = 4$. The structure is excited by a plane wave with normalized frequency $a/\lambda = 0.265$ and TE polarization. (b) Variation of the filtered out-of-plane electric field component (E_z) and its second derivative with position (x) along the guiding direction within a $\chi^{(3)}$ nonlinear bulk material with normalized $\chi^{(3)} = 4$. The structure is excited by a plane wave with normalized frequency $a/\lambda = 0.265$ and TE polarization.

Next, the transverse magnetic (TM) and TE field profiles for a slab of bulk $\chi^{(2)}$ material are shown in Fig. 5, where the normalized $\chi^{(2)} = 10$. TM is used to denote the field that only has a magnetic field component in the direction normal to the plane of the computational domain; TE denotes a field that only has an electric component in this direction. Note that in this simulation, we assume a very large value for $\chi^{(2)}$ to

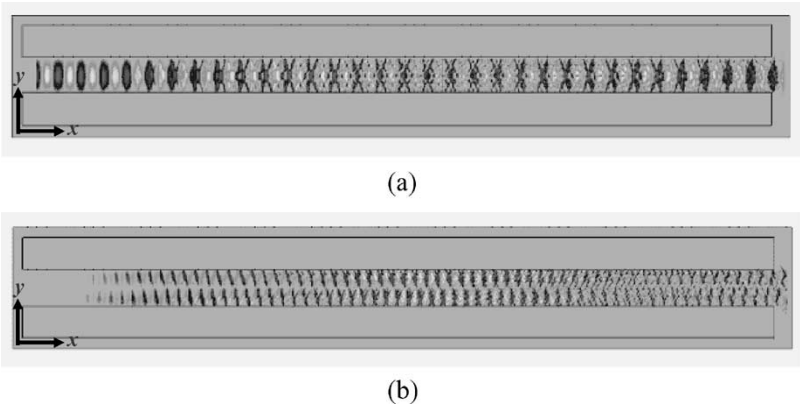

Fig. 5. SHG of a beam propagating in a dielectric slab waveguide by using a bulk $\chi^{(2)}$ nonlinear medium. The structure is a slab waveguide with dielectric core ($\varepsilon_r = 12.96$) and air cladding. The fundamental guided mode of the slab waveguide is excited using a Huygens' source, and the structure is surrounded by PML boundaries. (a) The spatial pattern of the magnetic field throughout the structure, used to pump the $\chi^{(2)}$ medium, as calculated by the nonlinear FDTD code. (b) The spatial pattern of the electric field throughout the structure, showing the generation of a second-harmonic beam in the $\chi^{(2)}$ medium.

reduce the required size of the computation domain. The TM field [Fig. 5(a)] is used to excite the material and the resulting nonlinear response initially shows up in the TE field [Fig. 5(b)], as predicted by expanding the matrix constitutive relationship assumed for the $\chi^{(2)}$ case (8). Again, an examination of the diagrams qualitatively indicates that a second-harmonic field is generated in the TE field (orthogonal to the TM excitation) and the energy is transferred periodically between the two, as expected. Of course, the energy conversion is not 100%, since there is a mismatch between the group velocities of the TE and TM polarizations due to waveguide dispersion. Furthermore, the null on the axis seen in the second-harmonic field [Fig. 5(b)] is due to the fact that the transverse magnetic field of the fundamental guided mode in the slab has even symmetry, and therefore, its electric field must vanish on the axis (i.e., the corresponding electric field has odd symmetry).

B. PC Structures

By applying nonlinear optics theory to PCs, we are able to take advantage of the additional control of light offered by both concepts. One benefit of using nonlinear effects is that the $\chi^{(3)}$ nonlinearity may be used to shift the phase of the guided modes in a controlled fashion, allowing for engineering of these modes in PC waveguides [62], [63]. Switching behavior can also be achieved by changing the strength of the nonlinearity of a material in the holes of a PC (e.g., by applying an electric field) if the bandgap of the PC disappears when the nonlinearity is large.

A related application uses the nonlinear phase shift to delay one optical pulse with respect to another. In this system, slow-light enhancement resulting from resonant structures can be used to increase the effects of the nonlinear material. This idea of enhancement using resonant structures can be developed further by using the guided modes of coupled resonator optical waveguides (CROWs), which can exhibit very small group velocities [25] primarily due to the coupling mechanism that allows light to gradually leak from one cavity to the next. A PC CROW with a cavity period of $\Lambda = 4a$ and made of dielectric rods is shown in Fig. 6(a), where a is the period of the bulk PC. The PC in this case is a square lattice of GaAs rods ($\varepsilon_r = 12.96$), having $r = 0.25a$, in a polymer background ($\varepsilon_r = 2.25$). The TE band structure of the bulk PC (no cavities) calculated using the linear FDTD code indicates a complete bandgap from about $a/\lambda = 0.237$ to 0.288. A point-defect cavity was created by decreasing the radius of the defect rod to $r' = 0.167$; the frequency response shows a resonant peak within the photonic bandgap (PBG) of the crystal near $a/\lambda = 0.264$ [Fig. 6(b)] and a change in amplitude and resonance shape when the defect rod is considered nonlinear ($\chi^{(3)} = 8$ used to exaggerate the effects). This resonance represents a defect cavity mode that becomes a guided CROW mode when several of these cavities are chained together. The dispersion diagram of the fundamental guided mode of this CROW is shown in Fig. 6(c). The relative flatness of the mode dispersion diagram indicates that this is, indeed, a low group velocity mode, given that the group velocity is directly related to the slope of the dispersion curve. As mentioned earlier, the small group velocity may be used to enhance the effects of a nonlinear material placed in these cavities, since the photons propagating through this structure spends a longer time in the nonlinear media than in a nonresonant waveguide of comparable length. The effective length of a given device L is directly proportional to the group velocity of light in the device v_G [33], as given by

$$\frac{L}{\lambda_{\text{air}}} \approx \frac{1}{2\sigma}\left(\frac{n}{\partial n}\right)\left(\frac{v_G}{c}\right). \tag{26}$$

Here, λ_{air} is the wavelength of light in air, ∂n is the induced index change created by nonlinear material, and σ represents the fraction of the energy localized in the region where ∂n is being applied. Thus, for smaller group velocities, the required device size shrinks. An application of slow-light enhancement is the Mach–Zehnder interferometer (MZI), shown in Fig. 7. In such a device, coherent light enters from the port on the left, light in one branch experiences a phase shift (φ) of $0 \leq \varphi \leq \pi$ with respect to the other branch, and then the light from both branches is recombined and allowed to interfere coherently. Thus, the light at the output on the right can vary from no light ($\varphi = \pi$) to full transmission ($\varphi = 0$), depending on the relative phase difference between the two arms. This concept may be implemented using a PC structure using the previous

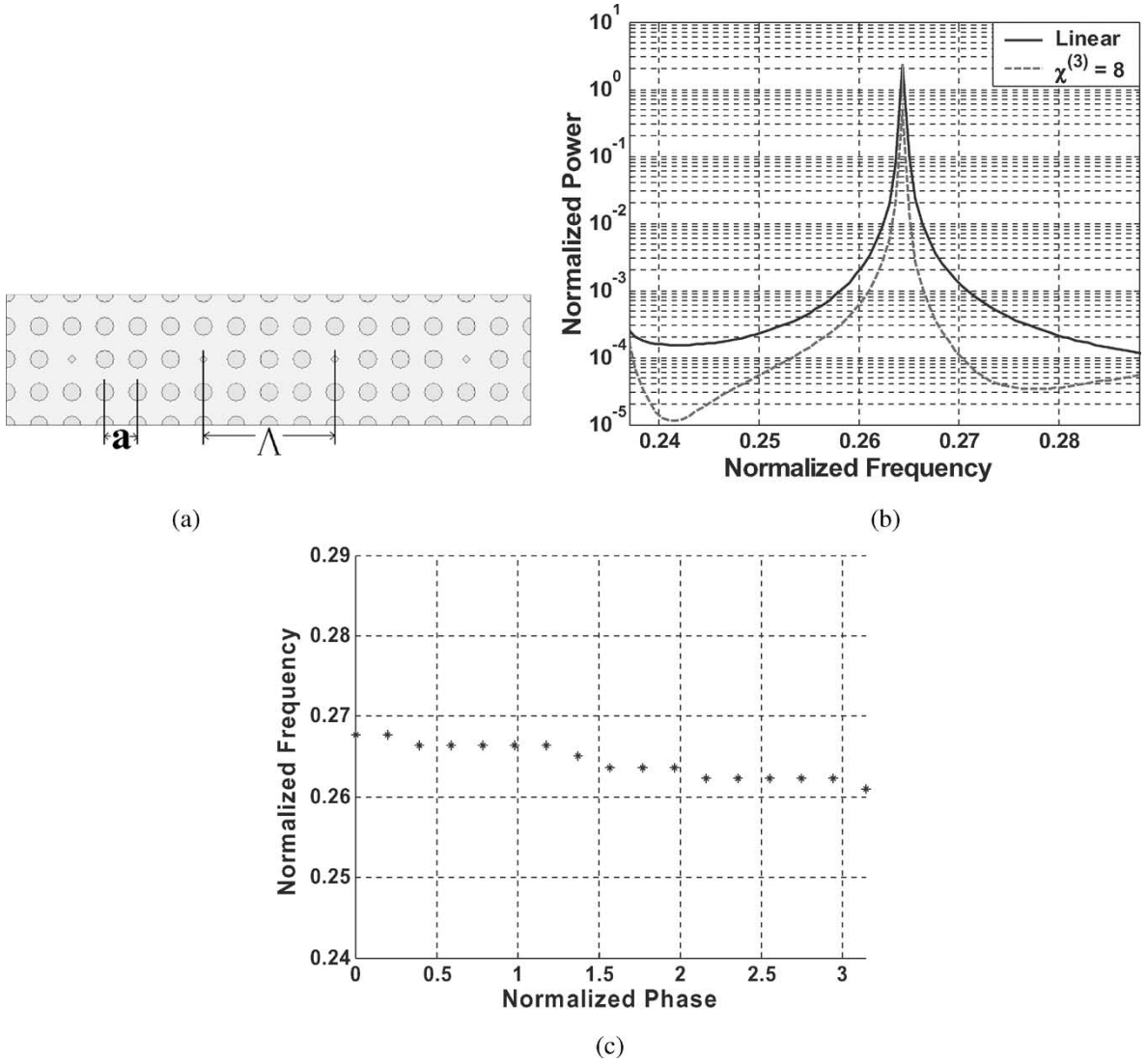

Fig. 6. (a) Square lattice PC CROW formed of GaAs rods, with $\varepsilon_r = 12.96$ and rod radius $r = 0.25a$, in a background of polymer ($\varepsilon_r = 2.25$); a is the lattice constant of the PC. The CROW was made by a periodic chain of point-defect cavities, where the cavity period $\Lambda = 4a$ and radius of the defect rod $r' = 0.167a$. (b) Frequency response around the bandgap of the PC cavity in Fig. 9(a) calculated using the linear FDTD method (solid) and nonlinear FDTD with $\chi^{(3)} = 8$ for the defect rod (dashed). (c) Dispersion diagram of the CROW calculated using the linear FDTD method.

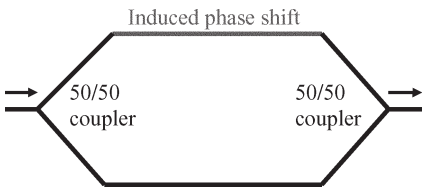

Fig. 7. Diagram of a single-drive MZI, where light enters from the left and is split between the two branches, with one branch producing a phase shift of $0 \leq \varphi \leq \pi$ with respect to the other branch. The light from both branches is recombined and allowed to interfere coherently at the output on the right.

rods-in-air CROW, where the phase shift is now induced using nonlinear effects.

The diagram in Fig. 8 shows this device, although the actual waveguides are difficult to distinguish due to the large overall size of the device. The numbers on the diagram indicate various points in the computational space where the power was recorded: 1 is at the input; 2 is near the middle of the lower waveguide branch; 3 is near the middle of the upper waveguide branch; and 4 is at the output. The plots in Fig. 9 show the power at each of these points at the end of the simulation (2^{17} time steps) for the linear and normalized $\chi^{(3)} = 0.5$, 1, and 2 cases (the field values were normalized to 3.5). Note that the x-axis has no physical significance; the numbers correspond to the numbered observation points within the structure (Fig. 8). Fig. 9 shows that some power is lost due to scattering in all of the simulations, but a decrease in optical power of as much as 11.7 dB (normalized $\chi^{(3)} = 0.5$) at the output is achieved by applying different values of normalized $\chi^{(3)}$. This may be attributed to the phase shift acquired by the light propagating in the upper waveguide as it passes through the nonlinear defect rods. Although these are preliminary results, they demonstrate appropriate operation of the device in that it correlates a phase shift between the upper and lower arms to an amplitude modulation at the output port. This simulation is presented primarily as validation of the nonlinear FDTD code in case of a rather complicated nonlinear structure and shows that the code is suitable for the analysis and optimization of such structures.

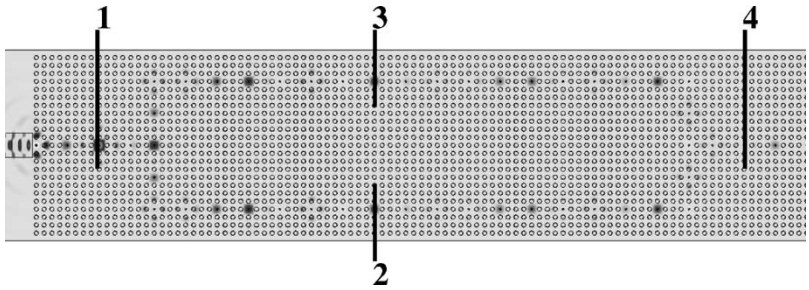

Fig. 8. Diagram of an MZI formed from the CROW shown in Fig. 6(a). Here, $\chi^{(3)}$ nonlinearity is applied to the defect holes ($r' = 0.167a$) in the upper branch of the MZI. The variation of the electric field calculated using the nonlinear FDTD method is also shown. The structure was excited by the fundamental TE mode of a dielectric slab waveguide (core $\varepsilon_r = 12.96$ and cladding $\varepsilon_r = 2.25$) on the left.

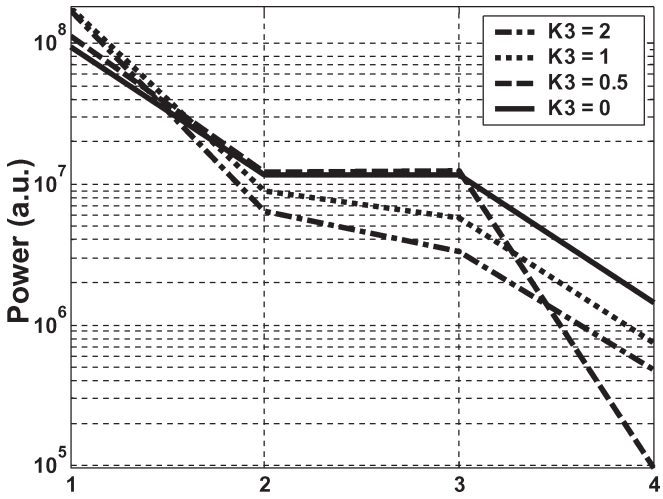

Fig. 9. Calculated power in CROW Mach–Zehnder structure using the nonlinear FDTD method at the four observation points shown in Fig. 8. The simulation was run for field values normalized to 3.5 and normalized $\chi^{(3)}$ values of 0 (solid line), 0.5 (dashed line), 1 (dotted line), and 2 (dot–dash line).

As a point of reference, an actual structure of this type designed for a wavelength of 1550 nm would have a lattice constant of $a = (1550\ \text{nm}) \times 0.265 \approx 411$ nm. With a total length of about $100a$, this structure would have an actual size of approximately $(411\ \text{nm}) \times 100 = 41.1\ \mu$m, as compared with typical values in the range of millimeters for a comparable planar waveguide structure and centimeters for a fiber-based system. Obviously, this reduced size combined with the possibility of integration using PC structures amounts to significant advantages over current technology in overall system size and power usage.

V. Conclusion

A nonlinear 2-D FDTD code based on a modification of the original Yee's FDTD algorithm that can simulate anisotropic, nonlinear $\chi^{(2)}$, and nonlinear $\chi^{(3)}$ materials of interest has been developed. The algorithm is stable under the Courant's stability condition, given that the strength of the nonlinear effect does not exceed a limit, which has been defined. The code has been verified using two applications that exhibit the well-understood phenomena of SHG and SPM in a bulk nonlinear medium. Finally, the operation of an MZI was simulated using phase shifting due to $\chi^{(3)}$ effects in a CROW structure, where the effective size of the device is greatly reduced compared to that of common devices of that type presently in use.

Acknowledgment

One of the authors (C. M. Reinke) thanks Lucent Technologies for their support in funding his graduate studies.

References

[1] R. W. Boyd, *Nonlinear Optics*. San Diego, CA: Academic, 1992.
[2] Y. S. Kivshar and G. Agrawal, *Optical Solitons: From Fibers to Photonic Crystals*. Boston, MA: Academic, 2003.
[3] C. Flytzanis and J. L. Oudar, *Nonlinear Optics: Materials and Devices*. Berlin: Springer-Verlag, 1986.
[4] D. L. Mills, *Nonlinear Optics*, 2nd ed. Berlin: Springer-Verlag, 1998.
[5] S. G. Johnson, S. Fan, P. R. Villeneuve, J. D. Joannopoulos, and L. A. Kolodziejski, "Guided modes in photonic crystal slabs," *Phys. Rev. B, Condens. Matter*, vol. 60, no. 8, pp. 5751–5758, Aug. 1999.
[6] M. Qiu, K. Azizi, A. Karlsson, M. Swillo, and B. Jaskorzynska, "Numerical studies of mode gaps and coupling efficiency for line-defect waveguides in two-dimensional photonic crystals," *Phys. Rev. B, Condens. Matter*, vol. 64, no. 15, pp. 155113–155117, Oct. 2001.
[7] S. Boscolo, C. Conti, M. Midrio, and C. G. Someda, "Numerical analysis of propagation and impedance matching in 2D photonic crystal waveguides with finite length," *J. Lightw. Technol.*, vol. 20, no. 2, pp. 304–310, Feb. 2002.
[8] P. Lalanne, "Electromagnetic analysis of photonic crystal waveguides operating above the light cone," *IEEE J. Quantum Electron.*, vol. 38, no. 7, pp. 800–804, Jul. 2002.
[9] T. Sondergaard, J. Arentoft, and M. Kristensen, "Theoretical analysis of finite-height semiconductor-on-insulator-based planar photonic crystal waveguides," *J. Lightw. Technol.*, vol. 20, no. 8, pp. 1619–1626, Aug. 2002.
[10] E. Lidorikis, M. L. Povinelli, S. G. Johnson, and J. D. Joannopoulos, "Polarization-independent linear waveguides in 3D photonic crystals," *Phys. Rev. Lett.*, vol. 91, no. 2, pp. 23902–23905, Jul. 2003.
[11] E. Yablonovitch, "Inhibited spontaneous emission in solid-state physics and electronics," *Phys. Rev. Lett.*, vol. 58, no. 20, pp. 2059–2062, May 1987.
[12] S. John, "Strong localization of photons in certain disordered dielectric superlattices," *Phys. Rev. Lett.*, vol. 58, no. 23, pp. 2486–2489, Jun. 1987.
[13] K. M. Ho, C. T. Chan, and C. M. Soukoulis, "Existence of a photonic gap in periodic dielectric structures," *Phys. Rev. Lett.*, vol. 65, no. 25, pp. 3152–3155, Dec. 1990.
[14] W. M. Robertson, G. Arjavalingam, R. D. Meade, K. D. Brommer, A. M. Rappe, and J. D. Joannopoulos, "Measurement of photonic band structure in a two-dimensional periodic dielectric array," *Phys. Rev. Lett.*, vol. 68, no. 13, pp. 2023–2026, Mar. 1992.
[15] K. W. K. Shung and Y. C. Tsai, "Surface effects and band measurements in photonic crystals," *Phys. Rev. B*, vol. 48, no. 15, pp. 1265–11269, Oct. 1993.
[16] A. Mekis, J. C. Chen, I. Kurland, S. Fan, P. R. Villeneuve, and J. D. Joannopoulos, "High transmission through sharp bends in photonic crystal waveguides," *Phys. Rev. Lett.*, vol. 77, no. 18, pp. 3787–3790, Oct. 1996.
[17] M. Loncar, M. Hochberg, A. Scherer, and Q. Yueming, "High quality factors and room-temperature lasing in a modified single-defect photonic crystal cavity," *Opt. Lett.*, vol. 29, no. 7, pp. 721–723, Apr. 2004.
[18] H. Takano, Y. Akahane, T. Asano, and S. Noda, "In-plane-type channel drop filter in a two-dimensional photonic crystal slab," *Appl. Phys. Lett.*, vol. 84, no. 13, pp. 2226–2228, Mar. 2004.

[19] S. F. Mingaleev and Y. S. Kivshar, "Nonlinear transmission and light localization in photonic crystal waveguides," *J. Opt. Soc. Amer. B, Opt. Phys.*, vol. 19, no. 9, pp. 2241–2249, Sep. 2002.
[20] J. D. Joannopoulos, R. D. Meade, and J. N. Winn, *Photonic Crystals: Molding the Flow of Light*. Princeton, NJ: Princeton Univ. Press, 1995.
[21] E. Yablonovitch, "Photonic crystals," *J. Mod. Opt.*, vol. 41, no. 2, pp. 173–194, 1994.
[22] S. John and M. Florescu, "Photonic bandgap materials: Towards an all-optical micro-transistor," *J. Opt., A Pure Appl. Opt.*, vol. 3, no. 6, pp. S103–S120, 2001.
[23] S. Fan and J. D. Joannopoulos, "Photonic crystals: Towards large-scale integration of optical and optoelectronic circuits," *Opt. Photon. News*, vol. 11, no. 10, pp. 28–33, 2000.
[24] J. Martorell, "Parametric nonlinear interaction in centrosymmetric three-dimensional photonic crystals," *J. Opt. Soc. Amer. B, Opt. Phys.*, vol. 19, no. 9, pp. 2075–2082, Sep. 2002.
[25] Y. Xu, R. K. Lee, and A. Yariv, "Propagation and second-harmonic generation of electromagnetic waves in a coupled-resonator optical waveguide," *J. Opt. Soc. Amer. B, Opt. Phys.*, vol. 17, no. 3, pp. 387–400, Mar. 2000.
[26] Y. Dumeige, I. Sagnes, P. Monnier, P. Vidakovic, C. Mériadec, and A. Levenson, "$\chi^{(2)}$ semiconductor photonic crystals," *J. Opt. Soc. Amer. B, Opt. Phys.*, vol. 19, no. 9, pp. 2094–2101, Sep. 2002.
[27] M. D. Rahn, A. M. Fox, M. S. Skolnick, and T. F. Krauss, "Propagation of ultrashort nonlinear pulses through two-dimensional AlGaAs high-contrast photonic crystal waveguides," *J. Opt. Soc. Amer. B, Opt. Phys.*, vol. 19, no. 4, pp. 716–721, Apr. 2002.
[28] M. Soljačić, M. Ibanescu, S. G. Johnson, J. D. Joannopoulos, and Y. Fink, "Optical bistability in axially modulated OmniGuide fibers," *Opt. Lett.*, vol. 28, no. 7, pp. 516–518, Apr. 2003.
[29] M. Soljačić, C. Luo, J. D. Joannopoulos, and S. Fan, "Nonlinear photonic crystal microdevices for optical integration," *Opt. Lett.*, vol. 28, no. 8, pp. 637–639, Apr. 2003.
[30] A. Babin and A. Figotin, "Nonlinear photonic crystals—I: Quadratic nonlinearity," *Waves Random Media*, vol. 11, no. 2, pp. R31–R102, 2001.
[31] ——, "Nonlinear photonic crystals—II: Interaction classification for quadratic nonlinearities," *Waves Random Media*, vol. 12, no. 4, pp. R25–R52, 2002.
[32] ——, "Nonlinear photonic crystals—III: Cubic nonlinearity," *Waves Random Media*, vol. 13, no. 4, pp. R41–R69, 2003.
[33] M. Soljačić, S. G. Johnson, S. Fan, M. Ibanescu, E. Ippen, and J. D. Joannopoulos, "Photonic-crystal slow-light enhancement of nonlinear phase sensitivity," *J. Opt. Soc. Amer. B, Opt. Phys.*, vol. 19, no. 9, pp. 2052–2059, Sep. 2002.
[34] D. Mihalache, F. Lederer, and D. M. Baboiu, "Two-parameter family of exact solutions of the nonlinear Schrodinger equation describing optical-soliton propagation," *Phys. Rev. A*, vol. 47, no. 4, pp. 3285–3290, Apr. 1993.
[35] E. L. Dawes and J. H. Marburger, "Computer studies in self-focusing," *Phys. Rev.*, vol. 179, no. 3, pp. 862–868, Mar. 1969.
[36] R. G. Beausoleil, W. J. Munro, and T. P. Spiller, "Applications of coherent population transfer to quantum information processing," *J. Modern Opt.*, vol. 51, no. 11, pp. 1559–1601, Nov. 2004.
[37] G. Fibich, B. Ilan, and S. Tsynkov, "Backscattering and nonparaxiality arrest collapse of damped nonlinear waves," *SIAM J. Appl. Math.*, vol. 63, no. 1, pp. 1718–1736, Feb. 2003.
[38] K. S. Yee, "Numerical solution of initial boundary value problems involving Maxwell's equations in isotropic media," *IEEE Trans. Antennas Propag.*, vol. AP-14, no. 3, pp. 302–307, May 1966.
[39] D. M. Sullivan, "Nonlinear FDTD formulations using Z transforms," *IEEE Trans. Microw. Theory Tech.*, vol. 43, no. 3, pp. 676–682, Mar. 1995.
[40] H.-H. Lee, K.-M. Chae, S.-Y. Yim, and S.-H. Park, "Finite-difference time-domain analysis of self-focusing in a nonlinear Kerr film," *Opt. Express*, vol. 12, no. 12, pp. 2603–2609, Jun. 2004.
[41] M. Bahl, N.-C. Panoiu, and R. M. Osgood, Jr., "Nonlinear optical effects in a two-dimensional photonic crystal containing one-dimensional Kerr defects," *Phys. Rev. B*, vol. 67, no. 5, pp. 56604-1–56604-9, May 2003.
[42] M. A. Alsunaidi, H. M. Masoudi, and J. M. Arnold, "A time-domain algorithm for the analysis of second-harmonic generation in nonlinear optical structures," *IEEE Photon. Technol. Lett.*, vol. 12, no. 4, pp. 396–397, Apr. 2000.
[43] A. Di Falco, C. Conti, and G. Assanto, *Terahertz Pulse Generation via Optical Rectification in Photonic Crystal Microcavities*, 2005. [Online]. Available: http://arxiv.org/abs/physics/0501065
[44] C. Conti, A. Di Falco, and G. Assanto, "Frequency generation within the forbidden band gap: All optical Rabi-like splitting in photonic crystals and microcavities," *Phys. Rev. E*, vol. 70, no. 6, pp. 66614-1–66614-5, Dec. 2004.
[45] ——, "Optical parametric oscillations in isotropic photonic crystals," *Opt. Express*, vol. 12, no. 5, pp. 823–828, Mar. 2004.
[46] ——, "Controlled transmission in the forbidden photonic bandgap via transient nonlinear states," *Opt. Lett.*, vol. 29, no. 24, pp. 2902–2904, Oct. 2004.
[47] A. Di Falco, "Wavelength shifting in photonic bandgap microcavities with isotropic media," *Appl. Phys. Lett.*, vol. 85, no. 20, pp. 4585–4587, Nov. 2004.
[48] P. Tran, "Optical switching with a nonlinear photonic crystal: A numerical study," *Opt. Lett.*, vol. 21, no. 15, pp. 1138–1140, Aug. 1996.
[49] ——, "Optical limiting and switching of short pulses by use of a nonlinear photonic bandgap structure with a defect," *J. Opt. Soc. Amer. B, Opt. Phys.*, vol. 14, no. 10, pp. 2589–2595, Oct. 1997.
[50] S. Visnovsky, R. Lopusnik, M. Bauer, J. Bok, J. Fassbender, and B. Hillebrands, "Magnetooptic ellipsometry in multilayers at arbitrary magnetization," *Opt. Express*, vol. 9, no. 3, pp. 121–135, Jul. 2001.
[51] R. M. Joseph and A. Taflove, "FDTD Maxwell's equations models for nonlinear electrodynamics and optics," *IEEE Trans. Antennas Propag.*, vol. 45, no. 3, pp. 364–374, Mar. 1997.
[52] A. Taflove and S. C. Hagness, *Computation Electrodynamics: The Finite-Difference Time-Domain Method*. Norwood, MA: Artech House, 2000.
[53] C. T. Chan, Q. L. Yu, and K. M. Ho, "Order-N spectral method for electromagnetic waves," *Phys. Rev. B*, vol. 51, no. 23, pp. 16635–16642, Jun. 1995.
[54] J. P. Berenger, "A perfectly matched layer for the absorption of electromagnetic waves," *J. Comput. Phys.*, vol. 114, no. 2, pp. 185–200, Oct. 1994.
[55] L.-X. Chen and D. Kim, "A bistable switching of two-dimensional photonic crystal with Kerr point defect," *Opt. Commun.*, vol. 218, no. 1–3, pp. 19–26, Mar. 2003.
[56] A. C. Cangellaris, "Numerical stability and numerical dispersion of a compact 2-D/FDTD method used for the dispersion analysis of waveguides," *IEEE Microw. Guided Wave Lett.*, vol. 3, no. 1, pp. 3–5, Jan. 1993.
[57] R. F. Remis, "On the stability of the finite-difference time-domain method," *J. Comput. Phys.*, vol. 163, no. 1, pp. 249–261, Sep. 2000.
[58] Y. Amnon and P. Yeh, *Optical Waves in Crystals: Propagation and Control of Laser Radiation*. New York: Wiley, 1984.
[59] V. Van and S. K. Chaudhuri, "A hybrid implicit-explicit FDTD scheme for nonlinear optical waveguide modeling," *IEEE Microw. Theory Tech.*, vol. 47, no. 5, pp. 540–545, May 1999.
[60] D. E. Merewether, R. Fisher, and F. W. Smith, "On implementing a numeric Huygen's source scheme in a finite difference program to illuminate scattering bodies," *IEEE Trans. Nucl. Sci.*, vol. NS-27, no. 6, pp. 1829–1833, Dec. 1980.
[61] T. Baba and T. Iwai, "Enhancement of third order nonlinearity calculated for two-dimensional photonic crystal," *Jpn. J. Appl. Phys.*, vol. 42, no. 4A, pp. 1603–1608, Apr. 2003.
[62] A. Adibi, Y. Xu, R. K. Lee, M. Loncar, A. Yariv, and A. Scherer, "Role of distributed Bragg reflection in photonic-crystal optical waveguides," *Phys. Rev. B*, vol. 64, no. 4, p. 041102, Jul. 2001.
[63] A. Adibi, Y. Xu, R. K. Lee, A. Yariv, and A. Scherer, "Guiding mechanisms in dielectric-core photonic-crystal optical waveguides," *Phys. Rev. B*, vol. 64, no. 3, p. 033308, Jul. 2001.

Charles M. Reinke (S'00) received the B.S. degree in physics from Jackson State University, Jackson, MS, in 2000 and the B.S.E.E. degree from the Georgia Institute of Technology, Atlanta, in 2001, after completing a dual-degree program. Currently, he is working toward the Ph.D. degree in electrical engineering from Georgia Tech, with an expected graduation date of May 2006.

He has participated in numerous summer internships with organizations such as Lucent's Bell Labs (from whom he is receiving his fellowship) and Lincoln Laboratory, Massachusetts Institute of Technology, Cambridge. During these programs, he worked on projects ranging from DWDM fiber component characterization, to Raman fiber amplification, to soliton pulse generation for high-speed communications networks. His current research projects involve measurement and characterization techniques for photonic crystal structures as well as studying the effects of nonlinear optical materials in photonic crystals. His technical interests include photonic integrated circuit technology, applications of quantum optical structures, and optical computing.

Aliakbar Jafarpour received the B.Sc. degree in electrical engineering with Highest Honor from Shiraz University, Shiraz, Iran, in 1997. He has been pursuing the Ph.D. degree at Georgia Institute of Technology, Atlanta, since 2001.

His areas of interests are photonic structures, nonlinear optics, and ultrafast optics.

Babak Momeni (S'02) was born in Tehran, Iran, in 1977. He received the B.Sc. and M.Sc. degrees in electrical engineering from Sharif University of Technology, Tehran, Iran, in 1999 and 2001, respectively. He is currently working toward the Ph.D. degree at the Georgia Institute of Technology, Atlanta.

His research interests include wave propagation in periodic structures, nonlinear optics, and analysis and applications of diffraction gratings.

Mr. Momeni is a Member of Eta Kappa Nu, the Optical Society of America (OSA), and the International Society for Optical Engineers (SPIE).

Mohammad Soltani received the B.Sc. and M.Sc. degrees in electrical engineering from Sharif University of Technology, Tehran, Iran, in 1999 and 2001, respectively. Since January 2002, he has been pursuing a Ph.D. degree with the electrical engineering program at Georgia Institute of Technology, Atlanta.

His general research interests are electromagnetics, quantum electronics, quantum optics, and condensed matter. His current research is on the design and fabrication of microcavities and coupled waveguide-cavities in photonic crystals for filtering and sensing, nonlinear optics in silicon microcavities, and slow wave structures.

Sina Khorasani was born in Tehran, Iran, on November 25, 1975. He received the B.Sc. and M.Sc. degrees in electrical engineering from Abadan Institute of Technology with the Highest Honour in July 1995 and Sharif University of Technology, Tehran, Iran, in February 1997. In the spring of 1996, he passed the Ph.D. entrance exam with the first rank and started his Ph.D. studies in optical electronics at Sharif University of Technology in February 1997, where he became an Assistant Professor immediately after receiving the Ph.D. degree in July 2001.

Since July 2002, he has been with the School of Electrical and Computer Engineering, Georgia Institute of Technology, Atlanta, as a research fellow. He has published over 20 journal papers and presented above 50 conference contributions in the fields of integrated optics and photonic crystals, plasma physics and magnetic confinement nuclear fusion, mathematical physics, numerical simulation, and electrochemistry.

Dr. Khorasani served as the General Chair for the IEEE International Millenium Seminar on Electrical Engineering, which was held on March 1–3, 2000, Tehran. He also has received a number of awards and honors, including the Best Paper Award at the Third National Energy Congress, Outstanding Ph.D. Graduate at Sharif University of Technology, and Postdoctoral Fellowship from Georgia Institute of Technology.

Ali Adibi (M'01–SM'03) received the B.S.E.E. degree from Shiraz University, Isfahan, Iran, in 1990 and the M.S.E.E. and Ph.D. degrees from Georgia Institute of Technology, Atlanta, in 1994 and California Institute of Technology, Pasadena, in 2000, respectively. His Ph.D. research resulted in a breakthrough in persistent holographic storage in photorefractive crystals.

He worked as a postdoctoral scholar at California Institute of Technology from 1999 to 2000 and joined Georgia Tech as an associate professor in 2000. His research interests include holographic data storage, holographic optical elements for optical communications; 3-D optical pattern recognition; design, characterization, and applications of photonic crystals for chip-scale WDM and biosensors; and optical communication and networking.

Dr. Adibi has been the conference chair for the "Photonic Crystal Materials and Devices" conference in Photonic West Meeting since 2001 and the program chair for the "Nanotechnology" program in Photonic West Meeting since 2002. He has served as a technical committee member for several conferences. He is the recipient of numerous awards including the Packard Fellowship (from the David and Lucile Packard Foundation), the NSF CAREER Award (from National Science Foundation), the SCEEE Young Faculty Development Award (from the Southeastern Center for Electrical Engineering Education), the NASA Space Act Award (from NASA), SPIE's Young Investigator Award, Outstanding Junior ECE Faculty Award (from Georgia Tech), the Howard Ector Outstanding Teacher Award (from Georgia Tech), the Richard M. Bass Outstanding Teacher Award (from Georgia Tech), the Charles H. Wilts Prize from Caltech (best EE thesis of the year), the New Focus Student Award from the Optical Society of America, the Top Student (D. J. Lowell) Award from SPIE, and the Oscar P. Cleaver Award from Georgia Tech (Outstanding EE graduate student of the year). He is a member of Sigma Xi, OSA, SPIE, and ASM.

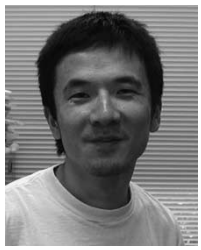

Yong Xu received the B.S. degree in applied physics from Tsinghua University, Beijing, China, in 1995 and the Ph.D. degree in physics from California Institute of Technology, Pasadena, in 2001.

His research interests are in the fields of novel photonic structures, fiber optics, nonlinear optics, and laser physics.

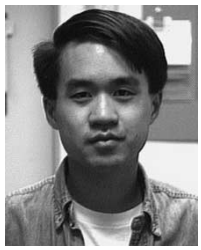

Reginald K. Lee (S'97–M'00) received the Bachelor of Applied Science degree in 1994 in aerospace engineering from the University of Toronto, Toronto, ON, Canada, and the M.S. degree in 1996 and the Ph.D. degree in 2000 in applied physics from the California Institute of Technology, Pasadena.

He is the Director of Product Development at Orbits Lightwave Inc. as well as a visiting research associate at the California Institute of Technology. He has conducted research in the areas of Fiber Bragg grating sensors and vertical cavity surface emitting lasers (VCSELs) and performed some of the first experimental work on active semiconductor photonic crystal structures. He also participated in the design, fabrication, and demonstration of the first lasing from a photonic crystal nanocavity: one of the worlds smallest semiconductor lasers. His current research interests include all-fiber devices, photonic crystals, and microresonators as well as narrow linewidth, ultra-stable low-noise fiber lasers for sensor and interferometry applications.